PAPER – 129 MATHEMATICAL MODELLING OF WELDING PARAMETERS AND THEIR EFFECTS ON ENERGY CONSUMPTION IN WELDED CR-MO METAL

Aweda J.O.[1] and Adewuyi, R.A.[2*]

[1]Department of Mechanical Engineering, University of Ilorin, Ilorin, Nigeria
[2]Department of Mechanical Engineering, The Federal Polytechnic, Ado-Ekiti, Nigeria
*Email: reuben1178@yahoo.com

ABSTRACT
This study examined the mathematical modelling of the effects of heat flux on welded Cr-Mo flat steel bars using the TIG arc welding method (ASTM A304). The TIG method employed was a double-sided half V-groove welding process with heat moving source while varying welding parameters such as material thickness, number of passes, electrodes' types and electric current in the process of welding. The mathematical transient heat transfer equations generated were run on Autodesk CFD 2018 software with welding parameters as inputs. The software was used to generate the 3-D model heat (temperature) profiles of the welded metal from the point of welding through the heat-affected zone to the parent metal. The temperature fields of the process produced by the software were distinguished by colours with the high intensity of heat being the welding zone (red) and the least at the parent metal (light blue). The temperature fields obtained were compared with the experimentally obtained values and found to be very close in values with the modelled values being slightly higher. The study demonstrated that modelling welding heat flux even before undertaking the process is a reliable tool to adopt in the welding of the Cr-Mo flat steel bar.

KEYWORDS**:** modelling, welding parameters, heat flux, electrodes.

1. INTRODUCTION

Welding is a widely used method in most fabrications for joining metals due to its reliability and effectiveness, Tailor *et al*. (2010). However, the failure rate of machine parts during service is significantly influenced by non-uniform volumetric temperature changes in welded specimens. Simulation tools based on finite element analysis (FEA) can predict weld heat cycles and stress analysis. Nevertheless, the current industrial practice still relies on trial and error and expertise from prior designs to develop welding procedures (Kollár & Kövesdi, 2018).

Previous literature has explored various aspects of Tungsten Inert Gas (TIG) welding's modelling, simulation and process optimization. Double ellipsoidal heat source model proposed by Goldak et al. (1984) was commonly used in welding simulation and has been shown to provide good agreement with results in the elastic-plastic analysis of welded plates. Additionally, the heat input and welding parameters strongly influenced the mechanical properties of weld joints. Zhu & Chao (2006) concluded that temperature-dependent material has significant effects on welding simulation in FEA. Both thermal and mechanical material properties should be considered temperature-dependent for accurate simulation. Thermal conductivity has some impact on the distribution of the transient temperature field during welding, but material density and specific heat have negligible effects. Rocha *et al*. (2018) investigated the modelling of the temperature field generated by the deposition of a weld bead on a steel butt joint by FEM techniques and thermographic images. The comparison of experimental and numerical results showed that the thermal cycles on all selected points were almost identical. However, in the cooling phase, there was a good agreement only until about 300°C. Both experimental and simulation methods were used for butt-welded specimens.

In this study, Autodesk Computational Fluid Dynamics (CFD) simulation software was utilized to analyse the thermal and stress effects of TIG welding on Cr-Mo steel bars of various thicknesses (5 mm, 10 mm, and 15 mm) measuring 50 mm by 100 mm. The impact of energy input, heat ad temperature distribution was examined and numerical analysis was validated with experimentally obtained transient temperature curves. The study aimed at evaluating the impact of weld heat input on the mechanical properties of Cr-Mo steel that was TIG welded and compared the results of Autodesk CFD simulation with the experimental results.

Therefore, simulation tools based on FEA have been used to predict weld heat cycles and temperature profiles of welded metal. This will lead to improvement in the accuracy of welding modelling with adequate prediction of both thermal and mechanical material properties of temperature.

2. METHOD OF SOLUTION

2.1. Numerical analysis

Finite Element Method (FEM) (Flint et al., 2017), a mathematical technique was adopted to solve the partial differential transient heat transfer equations generated during the welding operation. It was used to study and analyse complicated physical problems, particularly those displaying non-linear geometry and/or material behaviour, which is often the case in welding situations involving transient heat transfer. Some examples of coupled situations and conjugate heat transfer include thermomechanical, where confined differential thermal expansion causes thermal stresses and strains, and thermoelectric, where heat is generated in a material due to its resistance to current flow. Numerical setup for modelling of the transient state, the welding parameters and mechanical properties specified by ASTM A304 were considered. The model was created using Autodesk Inventor 2017 and then imported into Autodesk CFD 2018, where the mechanical properties were set to Cr-Mo steel bar A304 using the toolbar and the sequential modelling is presented in Table 1 and Figure 1.

Table 1: Mechanical Properties of Cr-Mo A304 Steel flat bar (Hashemzadeh et al., 2015)

Properties	Values
Density, ρ	8000 kg/m^3
Hardness	123 HV
Ultimate Tensile strength	505 MPa
Tensile strength at yield	215 MPa
Elongation at break	70 %
Modulus of elasticity	193–200 GPa
Poisson's Ratio	0.29
Charpy impact	325 J
Shear modulus	86 GPa

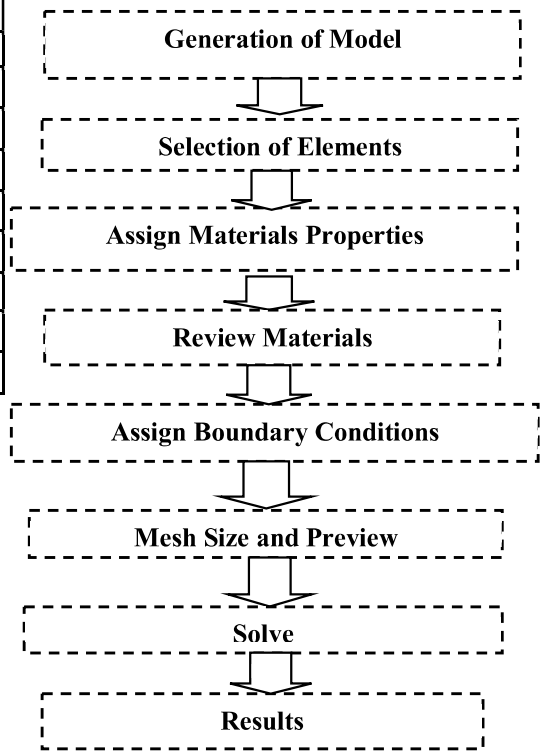

Figure 1: Sequential modelling

2.2. Experimental procedure

The Cr-Mo steel flat bar used was of varying thicknesses of 5mm, 10mm, and 15mm and was welded using a double-sided half V-groove joint with a Tungsten inert gas (TIG) welding machine. Other varying parameters include electrode diameter, weld current and number of weld passes. The materials were machined in pairs to size 100mm by 50mm from different thicknesses, with 18 samples of the Cr-Mo flat steel bar type under consideration. Before the welding operation, on each pair, a hole of 5.0 mm was drilled and tapped close to the weld centreline of the samples where a K-type thermocouple of 2000^{0}C capacity was connected to a data logger with type K thermocouples –3 channel–LU-MTM-380SD to measure temperature distribution between the base metal and welded bead which changes with time while welding operation was on. The Arc welding temperature (1350 - 1450 ^{0}C) was measured using Digital Infrared Thermometer Ametek LAND Cyclops 100L S/N 240671 91.

The assembly was performed with the welding current of 90 A, 100 A, and 150 A (DCEN), at a constant voltage of 24 V, and the welding rate of 0.2703 mm/s.

2.3. Theoretical analysis

The modelling of the transient state of a Tungsten Inert Gas (TIG) weldment using numerical and analytical methods is described in this study. A Double-Sided Half V-Groove weld joint that joins two steel bars was formed, with dimensions of 50mm by 100mm and thicknesses of 5mm, 10mm and 15mm. The welding procedure was modelled as a single pass on both sides of the bar in this analysis, and the weldment was symmetrical.

The Finite Element (FE) modelling of the TIG welding process was conducted in two steps using Autodesk Inventor 2017 for the physical modelling of the specimens and Autodesk CFD 2018 for structure and thermal analyses, the approach of Chujutalli et al. (2020), Ravinder (2015) and Rocha et al.(2018) were adopted and used in the validation. The non-uniform volumetric temperature distribution during the weld thermal cycle leads to non-uniform volumetric changes that cause weld thermal stresses. These non-uniform volumetric changes were due to solidification of the weld zone (WZ), metallurgical transformations, and plastic deformation, and result in distortion of grains. These welding-induced thermal stresses and distortion of grains are critical in the design of welded joints and structures. Figure 2 represented the numerical modelling of weld heat input with heat source Q adopted that focuses on the weld pool and Figure 3 shows heat conduction analysis in the weld metal. A finite element simulation was performed, yielding the temperature distribution, welding-induced thermal stresses and the distortion of grains in a Double-Sided Half V-Groove welded bar. Goldak's double ellipsoidal heat source model with Transient temperature distribution was used, following previous works by Tailor *et al*., 2010; Ravinder, 2015; Rocha *et al*., 2018; Hashemzadeh *et al*., 2015. The results of this study can be used to optimize the design and performance of welded joints and structures.

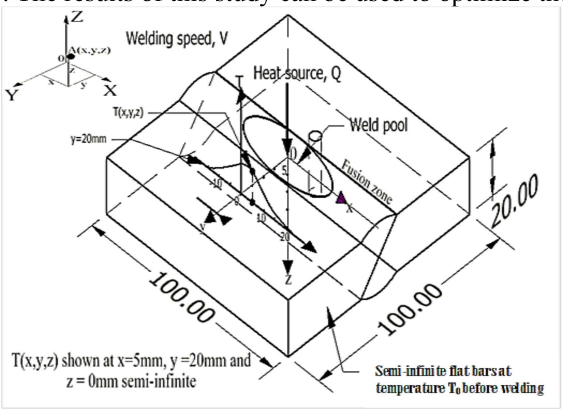

Figure 2: Weld heat input model in weld metal

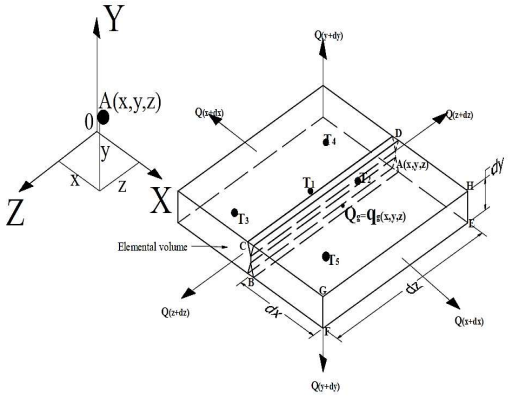

Figure 3: Heat conduction analysis in 3D model

Determination of Heat flux/thermal energy radiated over weldment surface, as shown in Figure 3. Heat flux/thermal energy over weldment surface (q): $Q/A=q= k\ dT/dx$ (1)

Where;

k =thermal conductivity of the material,

dT = change in temperature and dx = thickness of the material, according to Flint *et al.,* 2017, Trupiano *et al.,* 2022 and Rajput, 2012.

Let T = Temperature at the face ABCD (weld zone)

$(dT/dx)dx$ = Change in temperature through distance dx

$T+ (dT/dx)\ dx$ = temperature on the right face EFGH (at a distance dx from the left face ABCD; HAZ & Base metal).

2.4. Heat governing equations

Heat influx due to heat flow by conduction is given by the Fourier equation (Rajput, 2012)

$$Q'_x = -k_x(dy.dz)\frac{\partial T}{\partial x}.dt. \quad (2)$$

$$Q'_y = -k_y(dx.dz)\frac{\partial T}{\partial y}.dt. \quad (3)$$

$$Q'_z = -k_z(dx.dy)\frac{\partial T}{\partial z}.dt. \quad (4)$$

The transient temperature during welding is

$$\frac{\partial}{\partial x}\left[k_x\frac{\partial T}{\partial x}\right] + \frac{\partial}{\partial y}\left[k_y\frac{\partial T}{\partial y}\right] + \frac{\partial}{\partial z}\left[k_z\frac{\partial T}{\partial z}\right] + q_g = \rho.c.\frac{\partial T}{\partial t}. \quad (5)$$

or, using the vector operator ∇, we get

$$\nabla.(k\nabla T) + q_g = \rho.c.\frac{\partial T}{\partial t}. \quad (6)$$

The equations for convection and radiation are given as

$$q''_{conv} = h_f(T - T_0). \quad (7)$$
$$q''_{rad} = \varepsilon\sigma(T^4 + T_0^4). \quad (8)$$

Where

ρ = density, c = specific heat, q_g = internal heat generation rate, k = thermal conductivity and t =time interval. h_f =convection coefficient, ε = emissivity, σ = Stefan-Boltzmann constant, T = body temperature, and T_0 = ambient temperature, similar to observations by Hashemzadeh (2015) and Chen and Soares (2016).

2.5. Assumptions and boundary conditions

The heat transfer was in a transient state and involved several iterations between 0-500. The voltage used was 24V, the weld length was 100mm and the welding time was 370s. Based on experimental results, the welding rate was 0.2703mm/s.

2.6. Nodes, elements, degrees of freedom

Nodal discretization and Grid Independence test of nodes on peak temperature as shown in Figures 4 and 5 respectively. The 3D model of Cr-Mo flat steel bar underwent both thermal and structural analyses and had meshes consisting of 13,549 nodes and 6,989 elements (5 mm thick), 14,565 nodes and 7,537 elements (10 mm thick), and 16,254 nodes and 9,946 elements (15 mm thick) as represented in Figure 6(a-c). The degrees of freedom at each of the nodes that form the elements for thermal analysis is the temperature (T) and structural analysis is displacements (Ux, Uy, and Uz). The analysis at each node has four degrees of freedom - Ux, Uy, Uz, and T (due to thermal expansion effects) according to Arpita (2016), Malhotra *et al*. (2014) and Zhu and Chao (2006).

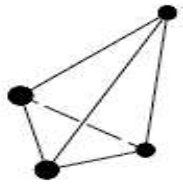

Figure 4: 3-D Solid element, Tetrahedral with four sides

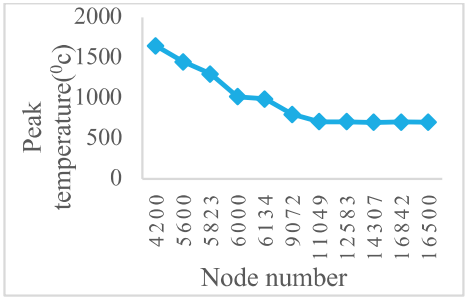

Figure 5: Grid Independence Test

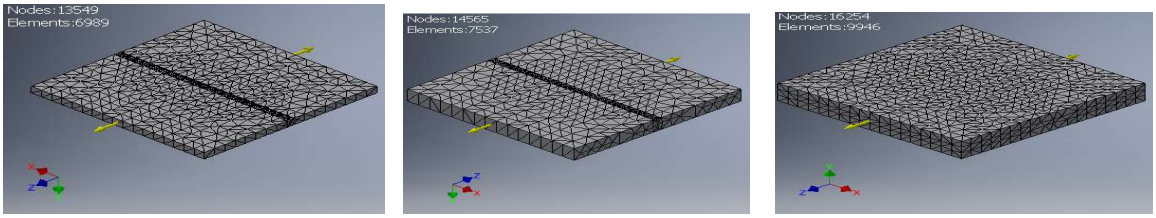

(a) (b) (c)

Figure 6(a-c): Geometry and mesh distribution in a 3D model for 5 mm, 10 mm and 15 mm thick Steel flat bars

3. RESULTS AND DISCUSSION

3.1 Thermal analysis of welded metal

The effect of weld heat input on welded metal was modelled with a coupled temperature-displacement analysis, each node in the weld model has three degrees of freedom Ux, Uy, Uz, and T (due to thermal expansion effects) in three planes (YZ, XZ, and XY). Thermal model (temperature fields) on Cr-Mo steel using Autodesk (CFD) 2018 revealed how temperature fields change over the length of the welded specimen. The reddish area of the weld zone changed towards the bar's edges. This colour change was used to investigate thermal stresses that occurred within the grains that lead to failure. The thermal simulation of the heat-affected zone and weld pool on Cr-Mo steel bar showing the three planes (YZ, XZ, XY) aids in understanding how differential heating and cooling in different zones of a weld

joint cause non-uniform volumetric changes, which lead to residual stresses. This type of data was useful for the determination of thermal stresses which normally lead to failure in machine parts. Figures (7-10) show the model result of weld heat input; one weld passes with 5mm, 90A, 1p & Ø1.6mm.

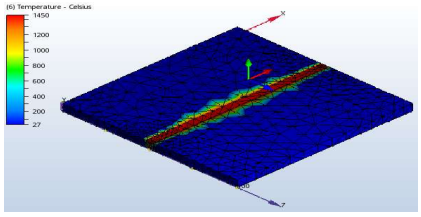

Fig. 7: 3-D Model generated

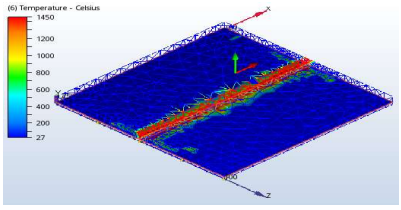

Fig. 8: Effect of weld heat input on HAZ across the Welded XZ plane along Y axis at 2.5 mm depth.

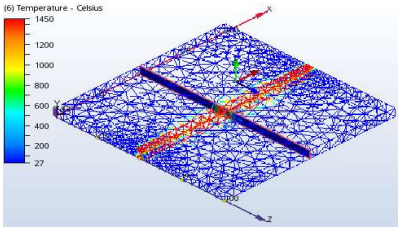

Fig. 9: Effect of weld heat input on HAZ welded area YZ plane along X axis 50 mm.

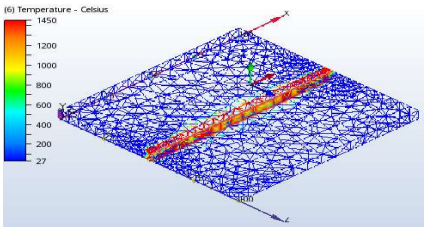

Fig. 10: Effect of weld heat input on HAZ on the welded area XY-plane along Z axis 5.2 mm away from weld centreline.

The variation of colours represented non-uniform volumetric changes in temperature at 3 mm depth below the surface of the bar. The different values of the temperature are shown in the figure. Figures (11-14) show the model result of weld heat input; one weld pass with 10 mm, 150 A, 1 p & Ø2.4 mm.

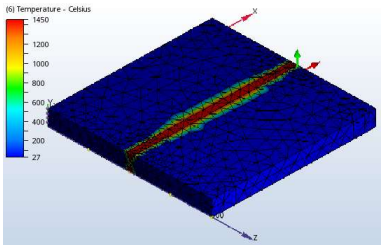

Fig.11: 3-D Model generated

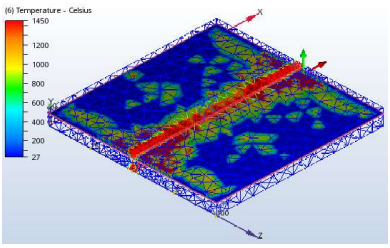

Fig. 12: Effect of weld heat input on HAZ across the welded XZ plane along Y axis at 3 mm depth

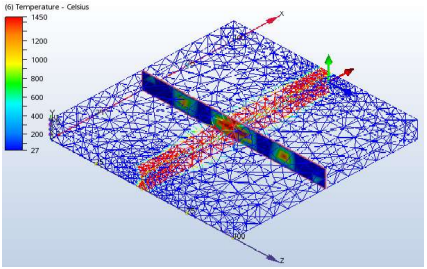

Fig. 13: Effect of weld heat input on HAZ on the welded area YZ-plane along X axis 50 mm.

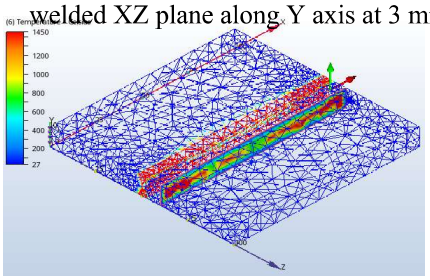

Fig. 14: Effect of weld heat input on HAZ along the welded area XY-plane along Z axis 10 mm away from weld centreline

The temperature profile of the xz-plane heat-affected zone away from the weld zone differs significantly from the bar's edges. The Figure shows non-uniform temperature distribution within the weldment away from the weld zone which altered the mechanical properties of the weldment leading to failure while in service. Figures (15-18) show the model result of weld heat input; two weld passes with 15 mm, 110 A, 1 p & Ø3.2 mm.

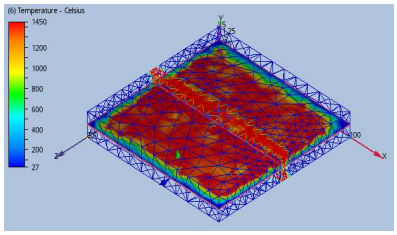

Fig. 15: 3-D Model generated

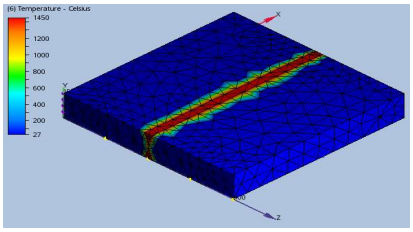

Fig. 16: Effect of weld heat input on HAZ across the welded XZ plane along Y axis at 7.5 mm depth

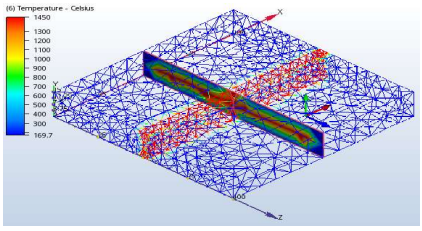

Fig. 17: Effect of weld heat input on HAZ on the welded area YZ-plane along X axis 50 mm.

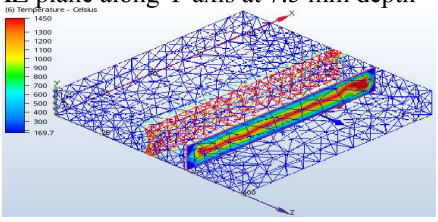

Fig. 18: Effect of weld heat input on HAZ along the welded area XY-plane along Z axis 20 mm away from weld centreline

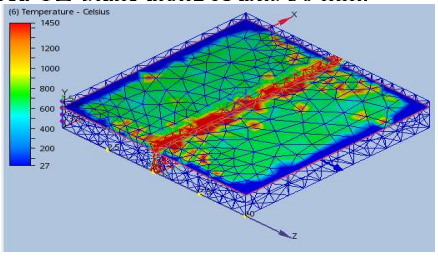

Fig.19: Effect of weld heat input on HAZ across the welded XZ-Plane along Y axis 3 mm depth.

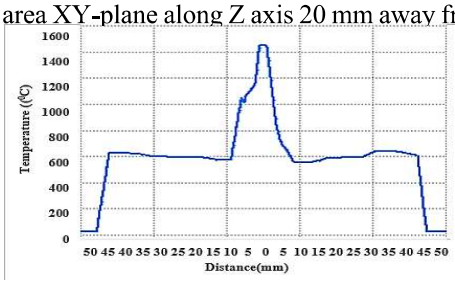

Figure 20: Temperature field against distances away from weld zone 3 mm depth.

Figure 19 illustrates non-uniform volumetric changes in temperature at 3 mm depth caused by cracks or slide lines, a material behaviour that causes the temperature to rise at some nodes/elements that form the mesh.
Tracing the nodes/elements that form the mesh on XZ-Plane across the weld zone revealed non-uniform volumetric changes in temperature presented in Figure 20. There is a decrease in temperature as it moves away from the weld zone

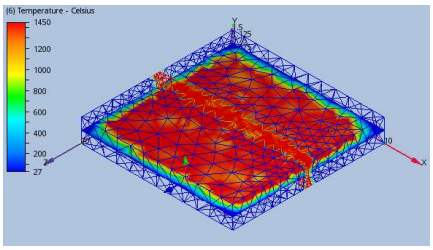

Figure 21: Effect of weld heat input on weldment XZ-Plane align to Y axis at 7 mm

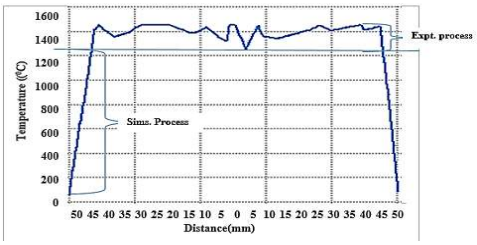

Figure 22: Temperature field against distances away from weld zone 7.5 mm depth.

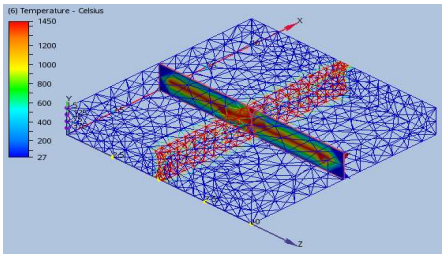

Figure 23: Effect of weld heat input on weldment at XZ-Plane along Y axis at 50 mm

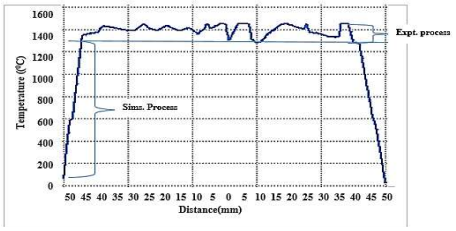

Figure 24: Temperature field against distances away from weld zone 5 mm depth.

Figures 19, 21 and 23 show the simulated welding curves and experimental welding curves which indicate the heating and cooling step on the surface of the bar, at 3 mm depth on the bar and 7.5 mm and on XZ-Plane along the Y axis at 50 mm on the bar within the weldment. The above graphs are obtained by picking nodes on the weldment which show the temperature distribution throughout the distance on the weldment. The temperature distribution obtained gradually increases to a max temperature of 1420^0C during the heating step and decreases to ambient temperature during the cooling step. Figures 20, 22 and 24 show the decrease in temperature as it moves away from the weld zone. Similar observations as reported by Cullen & Korkolis, 2013; Jelinek et al., 2020; Laser et al., 2017.

3.2. Effects of electrode diameter on heat flux

Figure 25 shows the effect of electrode diameter on Heat flux generated in the welded metal**.** The heat flux distribution obtained gradually decreases with an increase in metal thickness and electrode diameter.

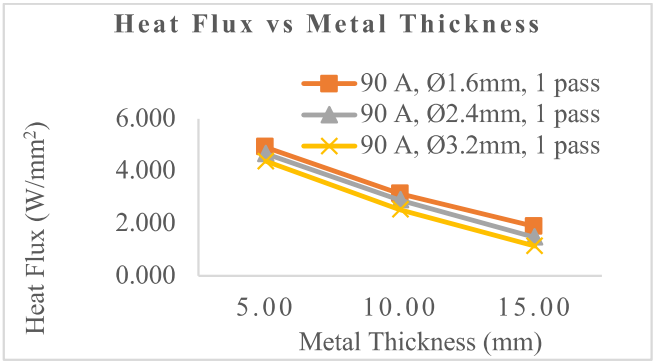

Fig. 25: Effect of Electrode diameter on Heat flux.

3.3. Effects of weld passes on heat flux

Figure 26 shows the effect of weld passes on Heat flux generated in the welded metal**.** The heat flux distribution obtained gradually decreases with an increase in metal thickness and the number of weld passes

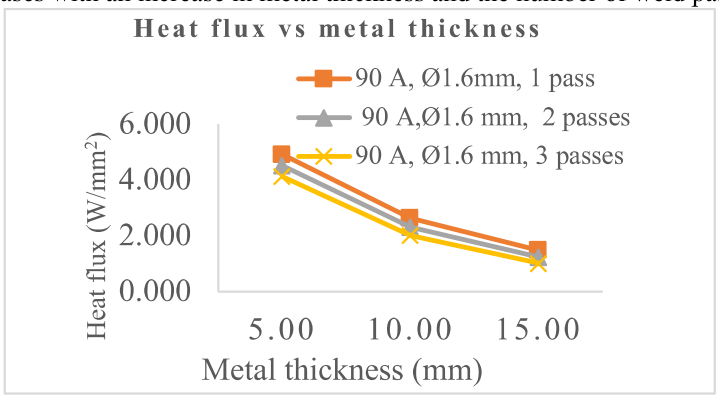

Fig. 26: Effect of weld pass on Heat flux.

3.4. Significant influence of welding parameters on heat flux

Figures 27(a-d) show the Regression Analysis with the equation as a function of Heat flux (W/mm2) versus welding parameters, which revealed that material thickness has a high significant influence on heat flux as shown in Figure 28a with a low standard deviation of 0.413816 compared to other welding parameters.

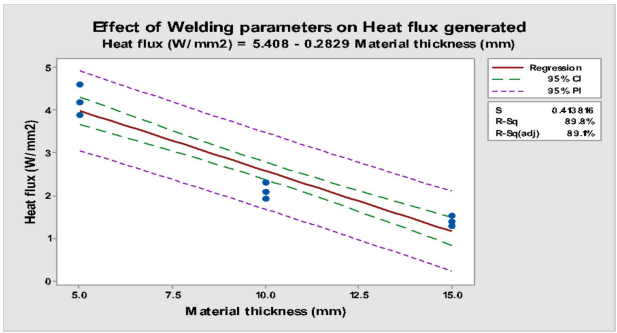

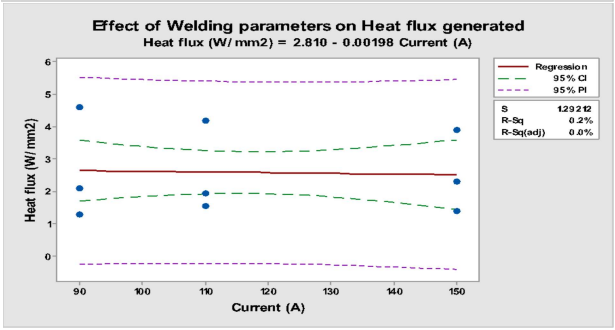

(a) (b)

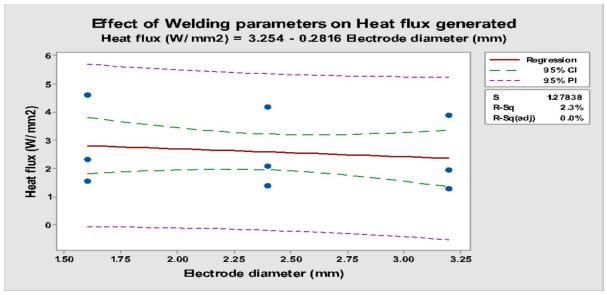

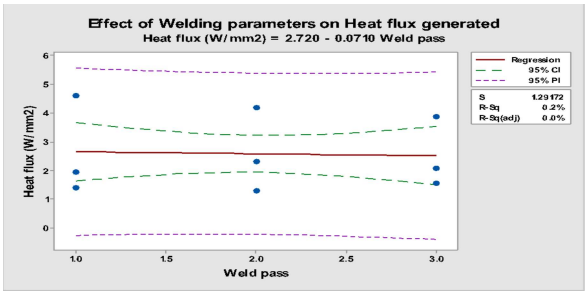

(c) (d)

Fig. 27(a- d): Effect of welding parameters on Heat flux generated in the weld metal

3.5 Typical Stress Analysis of welded metal

Von Mises stress distribution shown in Figures (28-33) was used to predict the yielding or failure of the material due to the load applied from uniaxial stress. The material experienced plastic deformation when the von Mises stress exceeded the yield strength. Based on the figures, the maximum von Mises stress plotted was 282.2 MPa (5 mm), 199 MPa (10 mm) and 158.43 MPa (15 mm) while the yield strength of the welded Cr-Mo Steel flat bar was 215MPa. Hence, the area with higher von Mises Stress above the Yield Strength experienced plastic deformation. The plastic deformation occurred mostly in the HAZ region.

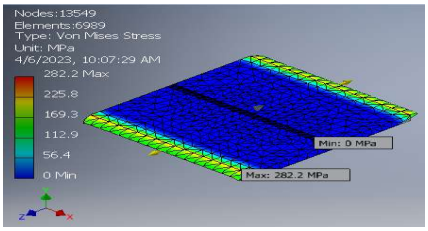

Fig. 28: Von Mises stresses on weld specimen

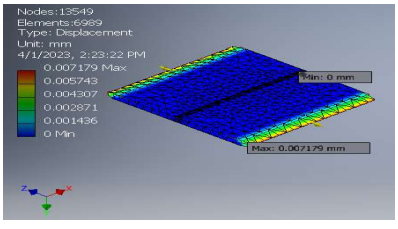

Fig. 29: Displacement on Weld Specimen

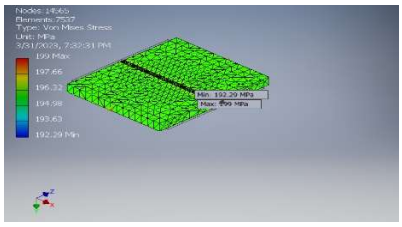

Fig. 30: Max.and Min. Von Mises stresses on welded specimen

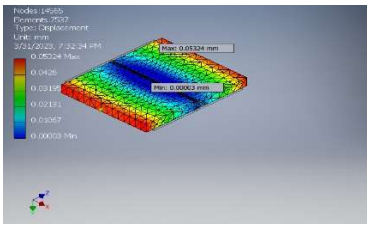

Fig. 31: Displacement on Weld Specimen

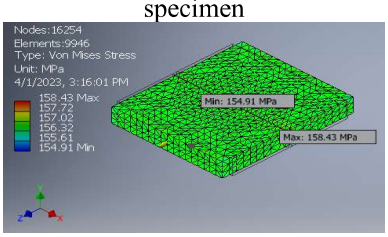

Fig. 32: Von Mises stresses on weld specimen

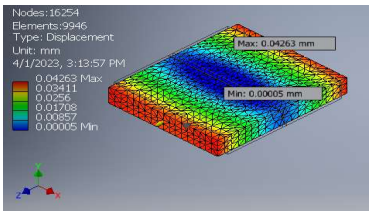

Fig. 33: Displacement on Weld Specimen

3.6 Comparison of numerical with experimental results

The variation in experimental and modelled mechanical properties of a welded Cr-Mo flat steel bar, concerning changes in material thickness and stress at break. It highlights the potential influence of factors such as increased residual stress and distortion in the weld region, changes in the microstructure of the material, and welding defects like porosity, cracking, or lack of fusion. Figures (34-35) emphasize the need to consider the specific parameters used in the model and their correspondence with the actual welding process used in the experiment. It also stresses the importance of accounting for variations in material properties, welding parameters, and testing conditions that could affect the results.

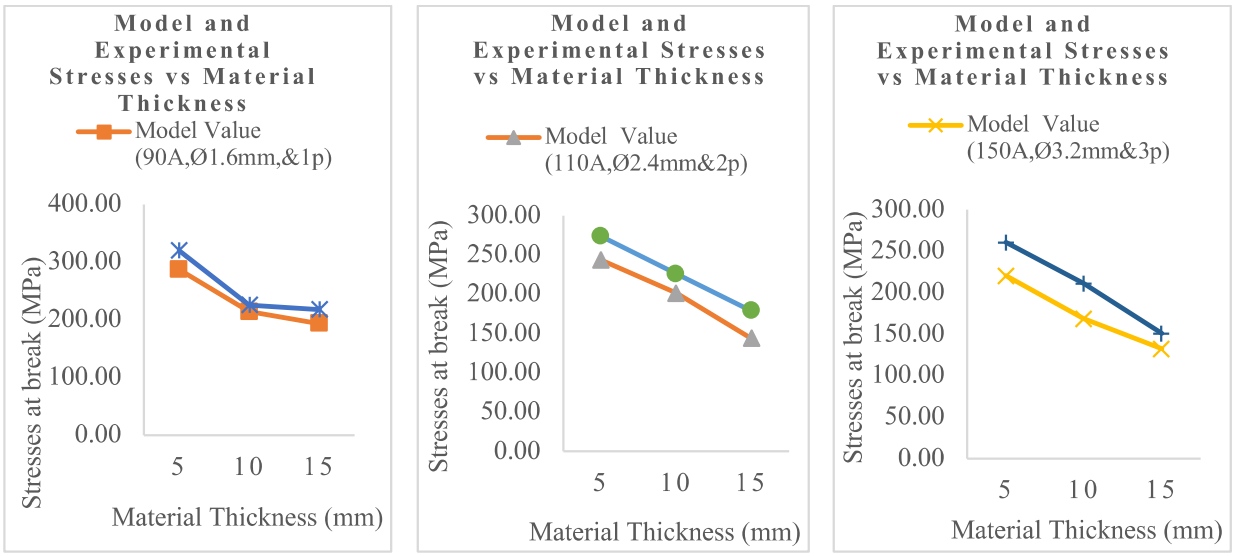

(a) (b) (c)

Fig. 34(a, b & c): Effect of weld parameters on stress in weld metal

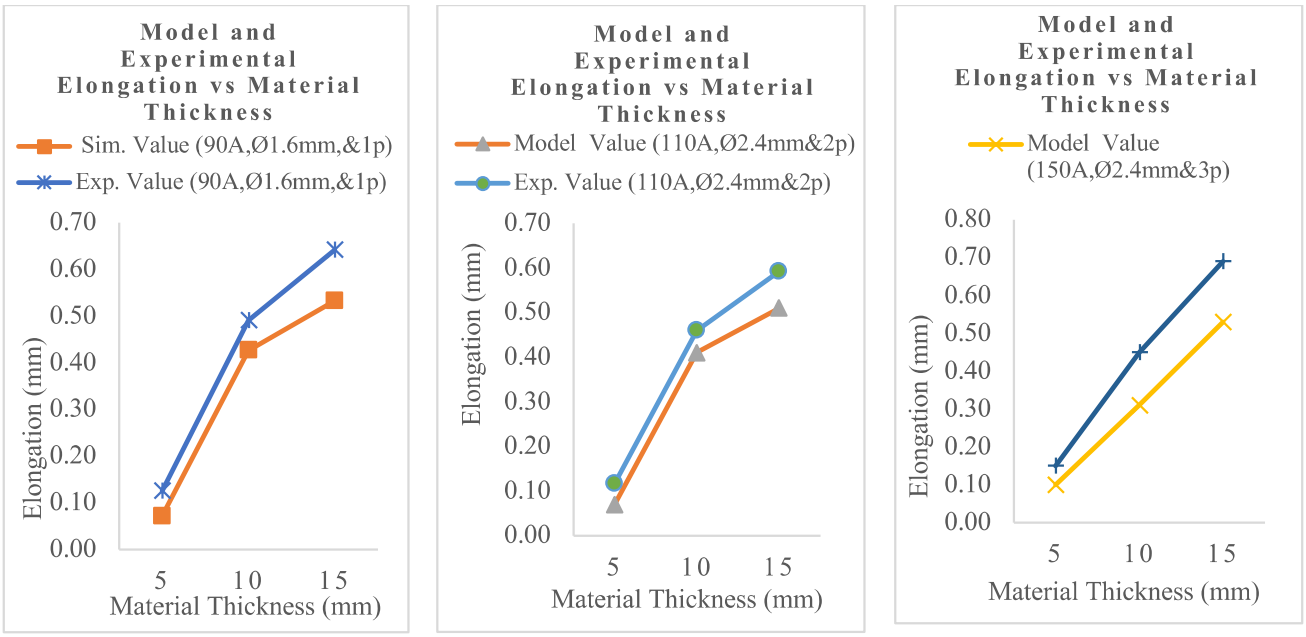

(a) (b) (c)

Fig. 35(a, b & c): Effect of weld parameters on Elongation in welded metal

3. CONCLUSIONS

It has been established that the Finite Element package, namely Autodesk Inventor and Autodesk CFD can be used to model weld heat input effect and predict material failure after the welding operation. The following specific conclusions can be drawn:

1. Von Mises stress follows tensile stress within 5-13% variation. FEA yields a safety factor of 10-12, indicating a safe design.
2. The optimum material thickness and welding current with high Von Mises stress are 5 mm and 90 A respectively.
3. Failure of fabricated machine parts can be predicted, based on the modelling results. Thus, the cost of experimental analysis can be avoided.
4. The material thickness has a great influence on the mechanical properties of the weld metal. An increase in the value of this parameter leads to a decrease in heat flux generated between 12.07 to 20.14%.

REFERENCE

Tailor, D. H., Srinivasan, K. N., Channiwala, S. A., Sohel, M., & Panwala, M. (2010). Simulation of temperature field of TIG welding using FDM. *American Society of Mechanical Engineers, Pressure Vessels and Piping Division (Publication) PVP*, *6*(PART A), 515–521. https://doi.org/10.1115/PVP2009-77697

Arpita N. Bhavsar, V. A. P. (2016). Influence of process parameters of TIG welding process on mechanical properties of SS304L welded joint. *International Research Journal of Engineering and Technology (IRJET)*, *03*(05), 977–984.

Chujutalli, J. H., Lourenço, M. I., & Estefen, S. F. (2020). Experimental-based methodology for the double ellipsoidal heat source parameters in welding simulations. *Marine Systems and Ocean Technology*, *15*(2), 110–123. https://doi.org/10.1007/s40868-020-00074-4

Flint, T. F., Francis, J. A., Smith, M. C., & Balakrishnan, J. (2017). Extension of the double-ellipsoidal heat source model to narrow groove and keyhole weld configurations. *Journal of Materials Processing Technology*, *246*(August), 123–135. https://doi.org/10.1016/j.jmatprotec.2017.02.002

Fu, G., Gu, J., Lourenco, M. I., Duan, M., & Estefen, S. F. (2015). Parameter determination of double-ellipsoidal heat source model and its application in the multi-pass welding process. *Ships and Offshore Structures*, *10*(2), 204–217. https://doi.org/10.1080/17445302.2014.937059

Hashemzadeh, M., Chen, B. Q., & Guedes Soares, C. (2015). Numerical and experimental study on butt weld with a dissimilar thickness of thin stainless steel plate. *International Journal of Advanced Manufacturing Technology*, *78*(1–4), 319–330. https://doi.org/10.1007/s00170-014-6597-6

Arpita N. Bhavsar, V. A. P. (2016). Influence of process parameters of TIG welding process on mechanical properties of SS304L welded joint. *International Research Journal of Engineering and Technology (IRJET)*, 03(05), 977–984.

Cullen, G. W., & Korkolis, Y. P. (2013). Ductility of 304 stainless steel under pulsed uniaxial loading. *International Journal of Solids and Structures*, 50(10), 1621–1633. https://doi.org/10.1016/j.ijsolstr.2013.01.020

Flint, T. F., Francis, J. A., Smith, M. C., & Balakrishnan, J. (2017). Extension of the double-ellipsoidal heat source model to narrow groove and keyhole weld configurations. *Journal of Materials Processing Technology*, 246(August), 123–135. https://doi.org/10.1016/j.jmatprotec.2017.02.002

Pu, X., Zhang, C., Li, S., & Deng, D. (2017). Simulating welding residual stress and deformation in a multi-pass butt-welded joint considering a balance between computing time and prediction accuracy. *International Journal of Advanced Manufacturing Technology,* 93(5–8), 2215–2226. https://doi.org/10.1007/s00170-017-0691-5

Reda, R., Magdy, M., & Rady, M. (2020). Ti – 6Al – 4V TIG Weld Analysis Using FEM Simulation and Experimental Characterization. *Iranian Journal of Science and Technology, Transactions of Mechanical Engineering,* 44(3), 765–782. https://doi.org/10.1007/s40997-019-00287-y

Rocha, E. J. F., De Sousa Antonino, T., Guimarães, P. B., Ferreira, R. A. S., Barbosa, J. M. A., & Rohatgi, J. (2018). Modelling of the temperature field generated by the deposition of weld bead on a steel butt joint by FEM techniques and thermographic images. *Materials Research,* 21(3). https://doi.org/10.1590/1980-5373-MR-2016-0796

Trupiano, S., Belardi, V. G., Fanelli, P., Gaetani, L., & Vivio, F. (2022). A semi-analytical method for the calculation of double-ellipsoidal heat source parameters in welding simulation. *IOP Conference Series: Materials Science and Engineering*, 1214(1), 012023. https://doi.org/10.1088/1757-899x/1214/1/012023